Inorganic Chemistry

Article

pubs.acs.org/IC

Combined High Resolution NMR and ^{1}H and ^{17}O Relaxometric Study Sheds Light on the Solution Structure and Dynamics of the Lanthanide(III) Complexes of HPDO3A

Daniela Delli Castelli,[†] Maria C. Caligara,[†] Mauro Botta,*[,‡] Enzo Terreno,[†] and Silvio Aime*[,†]

[†]Department of Molecular Biotechnology and Health Sciences, Molecular Imaging Center, University of Torino, Via Nizza 52, 10126 Torino, Italy

[‡]Dipartimento di Scienze e Innovazione Tecnologica (DiSIT), Università degli Studi del Piemonte Orientale "A. Avogadro", Viale T. Michel 11, I-15121 Alessandria, Italy

ABSTRACT: GdHPDO3A is one of the most used MRI contrast agents (CAs) for clinical use. However, unlike most of the other commercially available Gd-based CAs, only limited information is available on its solution structure and dynamics. 600 MHz high resolution ^{1}H NMR spectra of nine LnHPDO3A complexes (Ln = Pr, Nd, Eu, Tb, Dy, Ho, Er, Tm, and Yb) have been recorded at 298 K and neutral pH. Because of the low symmetry of the Ln-chelates, each proton gives rise to a different peak. Despite the very crowded spectra, it is possible to detect the presence of two sets of resonances associated with different isomers in solution in slow exchange in the NMR time scale. In principle, the LnHPDO3A complexes may be present in solution as eight isomeric forms (four enantiomeric pairs) differing in the layout of the acetate arms (Δ or Λ), in the conformation of the macrocyclic ring ($\delta\delta\delta\delta$ or $\lambda\lambda\lambda\lambda$) and in the configuration of the chiral center (R or S). 1D- and 2D proton NMR spectra were measured as a function of temperature across the Lanthanide series. The data allow identifying the nature of the most abundant isomeric species in solution (e.g., $\Lambda(\lambda\lambda\lambda\lambda)-R/\Lambda(\delta\delta\delta\delta)-R$ and their enantiomeric forms $\Delta(\delta\delta\delta\delta)-S/\Delta(\lambda\lambda\lambda\lambda)-S$) and their interconversion process. Analysis of the data led us to identify the presence in solution of a third isomeric species, lacking the coordinated water molecule ($q = 0$), whose population becomes more relevant for the heavier lanthanides (Ln = Er–Lu). Moreover, we have introduced an innovative way of modeling the thermodynamic equilibrium between the various isomeric forms of LnHPDO3A that can be extended to a number of other systems. This analysis enabled us to calculate the molar fractions of the two isomeric forms for GdHPDO3A ($\chi = 0.7$ and 0.30, for SAP and TSAP, respectively). This information has allowed interpreting the slightly anomalous relaxometric properties of GdHPDO3A. In particular, we observed that the temperature dependence of the ^{17}O NMR transverse relaxation rate of GdHPDO3A, R_2, reveals an unusual trend at low temperatures and at high magnetic field strength (>9.4 T). This behavior has been attributed to the occurrence of a very large difference in the rate of water exchange, k_{ex}, for the two isomeric species ($1/k_{ex} = \tau_M = 640 \pm 35$ ns and 8.9 ± 0.5 ns, for the major and minor isomer respectively).

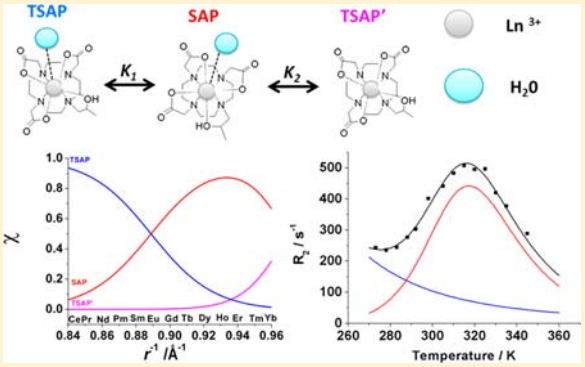

1. INTRODUCTION

The Gd-based MRI contrast agents have been used for nearly 30 years to improve the diagnostic information of the image and amplify the signal intensity.[1,2] Millions of examinations are performed annually worldwide with the use of these metal complexes. About 10 Gd(III)-complexes have been approved for clinical use, but over 800 have been proposed and investigated as potential MRI diagnostic probes. From the point of view of historical development and chemical-structural properties, four are the most important and well-known base systems: $[Gd(DTPA)(H_2O)]^{2-}$ (MAGNEVIST, Schering AG, DTPA = 1,1,4,7,7-pentakis(carboxymethyl)-1,4,7-triazaheptane), $[Gd(DTPA\text{-}BMA)(H_2O)]$ (Omniscan, Sanofi Nycomed, DTPA-BMA = 1,7-bis[(*N*-methylcarbamoyl)methyl]-1,4,7-tris-(carboxymethyl)-1,4,7-triazaheptane), $[Gd(DOTA)(H_2O)]^{-}$ (Dotarem; Guerbet, DOTA = 1,4,7,10-tetrakis-(carboxymethyl)-1,4,7,10-tetraazacyclododecane) and [Gd-(HPDO3A)(H_2O)] (ProHance Bracco, HPDO3A = 10-(2-hydroxypropy1)-1,4,7,10-tetraazacyclododecane-1,4,7-triacetic acid). Contrast agents are evaluated on the basis of their longitudinal proton relaxivities (r_{1p}, i.e., the increase in water proton relaxation rate per mM concentration of agent) that, for the clinically approved Gd(III) complexes, are in the range 4–5 mM^{-1} s^{-1}, at 0.47 T and 298 K.[3,4] Given the clinical relevance of this class of compounds, it is not surprising that their chemical properties have been the subject of detailed and thorough studies. The fundamental objectives of these studies are manifold: to understand in detail the relationship between the molecular parameters of the complexes and their ability to

Received: March 22, 2013
Published: June 5, 2013

dx.doi.org/10.1021/ic400716c | *Inorg. Chem.* 2013, 52, 7130–7138

accelerate the nuclear magnetic relaxation rate of water protons;[5−8] define the state of hydration of the metal ion;[9−11] check the possible existence of hydration equilibria or the presence of mixtures of stereoisomers;[12−14] verify the possible interactions with coordinating oxoanions or plasma proteins;[15] assess the stability of the complexes with respect to acid- or base-catalyzed dissociation.[16] Many of the studies dealt with metal ions other than Gd(III), exploiting the well-known similarity between the chemical-structural properties of the complexes of the lanthanide series and the diversity of their optical and magnetic properties.[17] This feature makes lanthanide chelates particularly suitable for investigation using a plurality of different experimental techniques. It is however quite surprising that while the knowledge acquired in relation to GdDTPA, GdDTPA-BMA, GdDOTA, and their derivatives is very detailed and thorough,[18,19] the information concerning GdHPDO3A is rather limited. Instead, the complexes of lanthanides with HPDO3A exhibit very interesting properties and are currently being investigated as effective diagnostic probes for various applications. For example, an analogue of this complex, namely, YbHPDO3A, has recently been proposed as a highly effective paramagnetic agent responsive to pH and temperature in the chemical exchange saturation transfer (CEST) way to generate contrast.[20] The close similarity of this compound with ProHance, in terms of stability and biodistribution, makes YbHPDO3A an optimal candidate as a first paraCEST probe suitable for the translation in clinical practice. A number of other applications in the field of MRI have been developed and reported, which require the use of LnHPDO3A complexes, for example as shift reagents for LipoCEST systems[21,22] or as T_2-susceptibility agents when encapsulated into liposomes.[23] Despite the great potential of these paramagnetic complexes, a study analyzing their structure in solution across the lanthanide series has not yet been addressed. In this work we have carried out a proton NMR study on several complexes of the lanthanide series, with the aim to further the knowledge on their solution structure and shed light on the number, nature and population of the different isomeric species. In this context, we have introduced an innovative way of modeling the thermodynamic equilibrium between the various isomeric forms of LnHPDO3A that can be extended to a number of other systems. In addition to these structural and dynamic issues, we have dealt with a detailed investigation to clarify the reasons for some small anomalies that can be found in the relaxometric properties of GdHPDO3A. In this regard, one can observe that the relaxivity of GdHPDO3A (r_{1p} = 4.60 ± 0.05 mM^{-1} s^{-1}; 20 MHz and 25 °C) is slightly lower than that of GdDTPA (r_{1p} = 4.80 ± 0.05 mM^{-1} s^{-1}) and GdDOTA (r_{1p} = 4.70 ± 0.05 mM^{-1} s^{-1}), measured under identical experimental conditions, in spite of their nearly identical molecular mass. It is well-established that, at high magnetic field (>0.2 T), the relaxivity of small Gd(III) complexes is determined predominantly from their rotational dynamics and thus by their molecular mass. Thus the slightly lower r_{1p} value reported for GdHPDO3A does not appear justified. Finally, we noticed that by measuring the temperature dependence of the ^{17}O NMR transverse relaxation rate of GdHPDO3A, R_2, an unusual trend is revealed at low temperatures and at high magnetic field (>9.4 T). Unlike the typical behavior observed for GdDTPA and GdDOTA, in the case of GdHPDO3A R_2 shows an increase by lowering temperature below about 280 K. Such behavior might suggest the existence in the aqueous solution of isomeric species with significantly different rates of water exchange. Interestingly, a significant difference between two diastereoisomers of GdHPDO3A in the magnitudes of the free-energy barriers for the water exchange has recently been suggested using ab initio simulations.[24,25] We have checked this hypothesis by reanalyzing the relaxometric data in terms of a two-species model. The results of this study show the high level of detail that can be achieved in defining the structural and dynamic characteristics of paramagnetic lanthanide(III) complexes in solution through the combined use of multifrequency and multinuclear NMR techniques at high and low resolution.

Chart 1. Chemical Structures of the Ln(III) Complexes with the Macrocyclic Ligands DOTA and HPDO3A

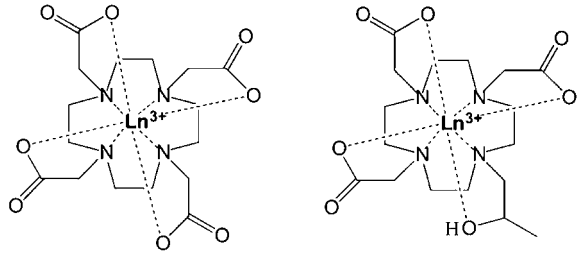

[Ln(DOTA)]⁻ Ln(HPDO3A)

2. EXPERIMENTAL SECTION

2.1. Sample Preparation. The racemic form of the ligand HPDO3A has been kindly provided by Bracco Imaging S.p.A. LnHPDO3A complexes have been prepared by mixing in a stoichiometric ratio the lanthanide oxide and the ligand (allowing for 1−2% ligand excess to avoid free metal ions) in water. The reaction mixture was stirred and heated at 80 °C until a clear solution was obtained. The reaction time depends strongly on the lanthanide ion. The final solution was filtered and the solvent evaporated under reduced pressure.

For all the NMR and relaxometric measurements, the concentration of the aqueous solutions of the Ln-complexes was determined by measuring the bulk magnetic susceptibility[26] on a Bruker Avance 600 spectrometer (14 T). To this end, 10% (v/v) of *tert*-butyl alcohol was added to a small aliquot of the stock solutions. The absence of free lanthanide(III) ions was verified using xylenol orange as indicator.

2.2. NMR Measurements. *^1H NMR.* The complexes were dissolved in D_2O, and the pD was adjusted to 7.4 (pH = 7.0) by addition of DCl or KOD and checked with a glass electrode connected to an As instruments pH-meter. The spectra were recorded at 14.1 T on a Bruker Avance 600 spectrometer. The temperature was controlled with Bruker thermostatting units, and high resolution spectra have been acquired by varying the temperature from 278 to 350 K. EXSY spectra were collected by using the standard NOESY pulse sequence (90°-t_1-90°-τ_M-90°) where the mixing time τ_M has been set to 5 ms. To assign mobile proton signals, LnHPDO3A solutions either in H_2O or D_2O at pH 5.0 have been prepared, and their NMR spectra have been compared. Lanthanide induced shift on bulk water have been measured by correcting for susceptibility effect using *tert*-butyl alcohol as a reference. The molar fractions were calculated from peak areas (integration). The Ln(III) ionic radius has been taken after Shannon for coordination IX.[27]

^1H and ^{17}O NMR Relaxometric Measurements. The water proton longitudinal relaxation rates were measured on about 0.5−1.5 mM solutions of the Gd(III) complex in nondeuterated water. The $1/T_1$ NMRD profiles were measured on a fast field-cycling Stelar SmartTracer relaxometer (Stelar s.r.l., Pavia, Italy) over a continuum of magnetic field strengths from 0.00024 to 0.25 T (corresponding to

dx.doi.org/10.1021/ic400716c | Inorg. Chem. 2013, 52, 7130−7138

0.01−10 MHz proton Larmor frequencies). The relaxometer operates under computer control with an absolute uncertainty in $1/T_1$ of ±1%. The temperature was controlled with a Stelar VTC-91 airflow heater equipped with a calibrated copper−constantan thermocouple (uncertainty of ±0.1 K). Additional data points in the range 15−70 MHz were obtained on a Stelar Relaxometer equipped with a Bruker WP80 NMR electromagnet adapted to variable-field measurements (15−80 MHz proton Larmor frequency). Variable-temperature ^{17}O NMR measurements were recorded on a Bruker Avance 600 spectrometer (14.1 T) equipped with a 5 mm probe and standard temperature control unit. Aqueous solutions of the complex (10−20 mM) containing 2.0% of the ^{17}O isotope (Cambridge Isotope) were used. The observed transverse relaxation rates were calculated from the signal width at half-height. The bulk magnetic susceptibility contribution was subtracted from the ^{17}O NMR shift data using the ^1H NMR shifts of the ^{t}BuOH signal as internal reference.

3. RESULTS AND DISCUSSION

3.1. Solution NMR. HPDO3A is a macrocyclic polyaminocarboxylic ligand that differs from the well-known DOTA chelator for the substitution of a pendant acetate arm with a hydroxypropyl moiety. Octadentate polyaminocarboxylate chelates such as DOTA are able to encapsulate the central lanthanide ion between the four coplanar nitrogen atoms of the macrocyclic ring and the four coplanar oxygen atoms of the acetic pendant arms. A ninth coordination position is occupied by a water molecule in a capping axial position. The macrocyclic ring in $[Ln(DOTA)]^-$ complexes can exist in two different coordination geometries. A larger torsion angle (39°) between the two square planes defines a capped square antiprismatic geometry (SAP), whereas a smaller torsion angle (25°) is associated with a capped twisted square antiprism (TSAP) in which the orientation of the acetate arms is rotated.[28] These isomers mutually exchange in solution, and the interconversion proceeds either through inversion of the macrocyclic ring conformation or by rotation of the four acetic groups.[29,30] Two different conformations may be envisaged for an ethylene bridge in a macrocycle, namely, λ or δ according to the sign of the torsion angle. Hence, the conformation of the macrocycle in DOTA-like complexes may be either ($\delta\delta\delta\delta$) or ($\lambda\lambda\lambda\lambda$). Moreover, the pendant arms may be oriented clockwise (Δ) or anticlockwise (Λ). It follows that four isomers (two enantiomeric pairs) can be present in solution: $\Delta(\lambda\lambda\lambda\lambda)/\Lambda(\delta\delta\delta\delta)$ (SAP) and $\Delta(\delta\delta\delta\delta)/\Lambda(\lambda\lambda\lambda\lambda)$ (TSAP). Combined rotation of the arms and ring inversion determines the interconversion between the enantiomers.[31] The solution structure of $[Ln(DOTA)]^-$ chelates has been extensively investigated by high resolution NMR spectroscopy. Proton spectra show the presence of 12 peaks divided in two groups of six assigned to the SAP or TSAP isomers, respectively. These previous results form the basis for interpreting the NMR spectra of the Ln(HPDO3A) system. The 600 MHz high resolution ^1H NMR spectra of nine Ln(HPDO3A) complexes (Ln = Pr, Nd, Eu, Tb, Dy, Ho, Er, Tm, and Yb) have been acquired at 278 K and pH 7.0 (Figure 1). It is worth noting that the replacement of one acetic group for a hydroxypropyl moiety determines the loss of the C4 symmetry and removes the equivalence among the protons of the ligand. So, the spectra of the LnHPDO3A complexes are highly crowded and more difficult to analyze. In spite of this problem, it is possible to observe the presence of two sets of 25 NMR resonances (Figure 1a) differing in their relative abundance.

This indicates the coexistence of at least two isomeric species in solution that are in slow exchange on the NMR time scale. In

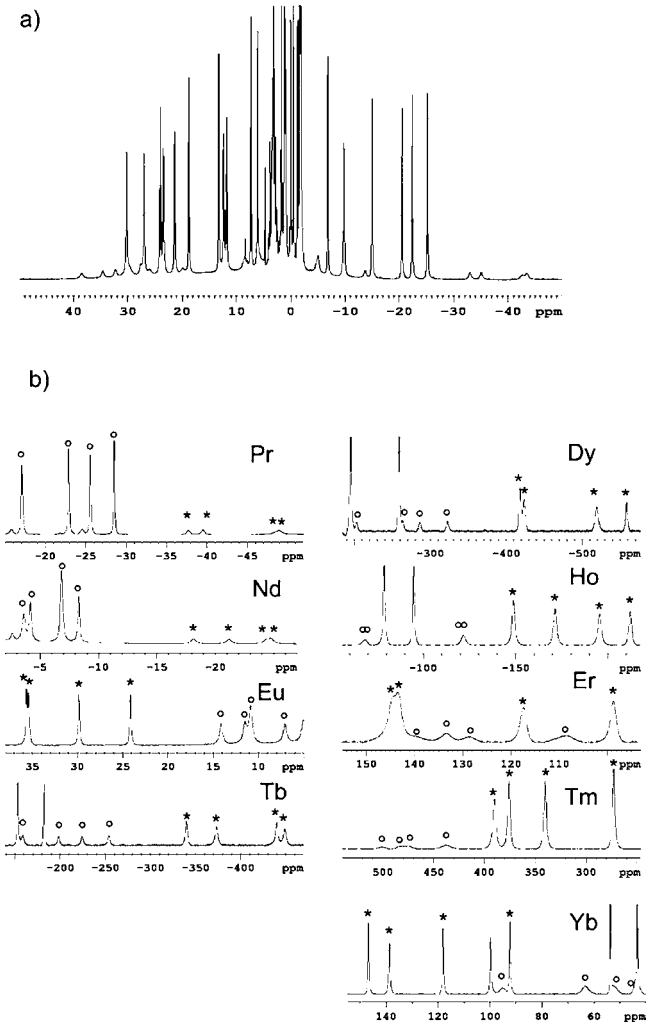

Figure 1. (a) 600 MHz ^1H NMR spectrum of PrHPDO3A; (b) portion of the NMR spectrum showing the region of the axial protons for both the isomer SAP (*) and TSAP (○) of the nine LnHPDO3A complexes. All the spectra have been measured at 278 K and pD = 7.4 (pH = 7.0).

principle, the macrocyclic Ln(HPDO3A) complexes may be present in solution as eight isomeric forms differing in the layout of the acetate arms (Δ or Λ), in the conformation of the macrocyclic ring ($\delta\delta\delta\delta$ or $\lambda\lambda\lambda\lambda$), and in the configuration of the chiral center (*R* or *S*). Among these eight isomeric structures those differing either in the configuration of the chiral center, in the layout of the acetate arms, and in the conformation of the macrocyclic ring originate enantiomeric pairs while the others represent diasteroisomers (Scheme 1a). Because the complexes were synthesized starting from a racemic ligand, each resonance in the NMR spectrum corresponds to a 50% mixture of the *R* and *S* enantiomers.

Unlike the $[Ln(DOTA)]^-$ complexes, the Ln(HPDO3A) enantiomers cannot interconvert with each other because they differ in the configuration of the chiral carbon. The solution dynamics of the eight diasteroisomers is graphically represented in Scheme 1b. The X-ray structure of Gd(HPDO3A)[32] shows in the unit cell the presence of both SAP and TSAP forms. Tweedle and co-workers reported that crystallization occurs with "spontaneous resolution" of the racemic mixture resulting in a conglomerate containing equal amounts of *R* and *S* crystals. The asymmetric unit contains two crystallographically

dx.doi.org/10.1021/ic400716c | Inorg. Chem. 2013, 52, 7130−7138

Scheme 1. (a) Four Enantiomeric Pairs of the Ln(HPDO3A) Complexes,[a] and (b) Interconversion Pathways among the Eight Stereoisomers

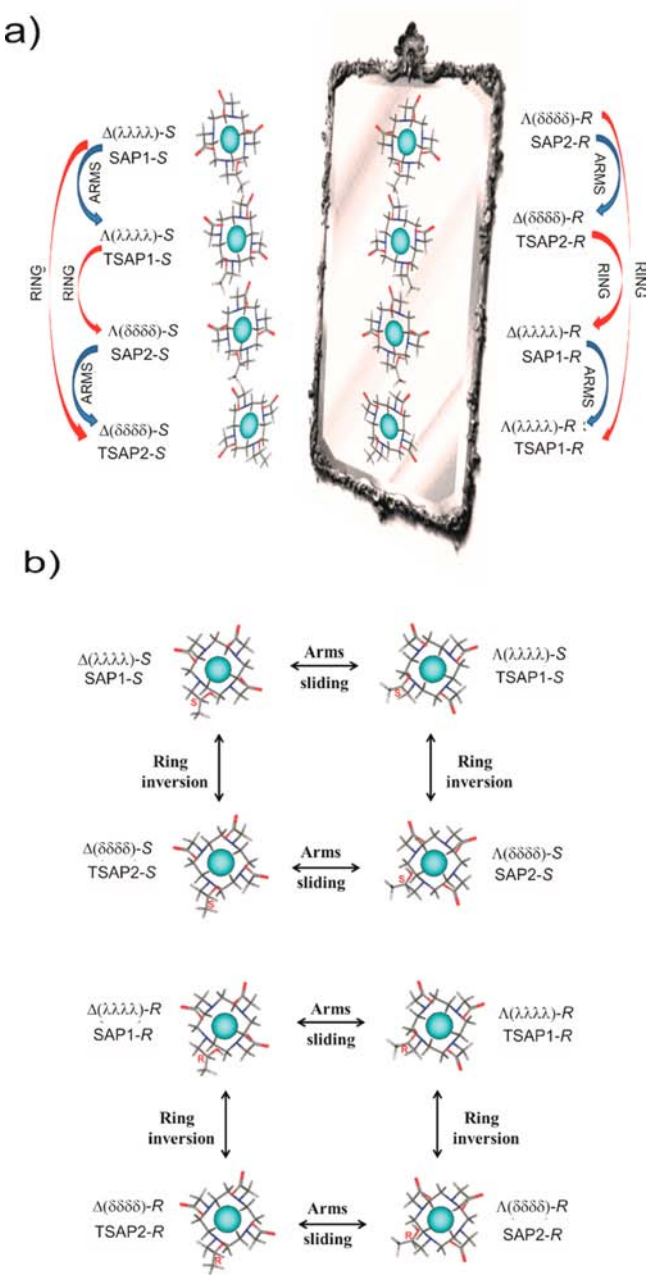

[a]Red arrows connect isomers interconverting through the inversion of the ring, blue arrows connect isomers interconverting through the rotation of the arms.

independent molecules of the complex sharing the same configuration of the chiral center. The two independent complexes in the asymmetric unit have diastereomeric conformations. Thus, the four coordinating arms are all twisted in the same sense, while the quadrangular conformations of the tetraazacyclododecane ring are enantiomeric. The two independent complexes correspond to the isomeric forms $\Lambda(\lambda\lambda\lambda\lambda)$-*R* (TSAP1-*R*) and $\Lambda(\delta\delta\delta\delta)$-*R* (SAP2-*R*). A first objective of this study is to verify if the diasteroisomers identified at the solid state correspond to those observed in the solution NMR spectra. Given the strong structural analogy between the Ln(HPDO3A) and $[Ln(DOTA)]^-$ complexes, the most shifted set of protons peaks in the NMR spectra have been assigned to the isomer corresponding to the SAP geometry, whereas the less shifted group has been attributed to the TSAP isomer. As previously found for $[Tm(DOTA)]^-$, also in the case of Tm(HPDO3A) this assignment is reversed. To get more insight into the solution structure and dynamics of the isomeric forms, ^{1}H NMR spectra have been recorded as a function of temperature and 2D EXSY maps acquired at 298 and 278 K for the complexes of Pr^{III}, Nd^{III}, and Eu^{III} (Figure 2).

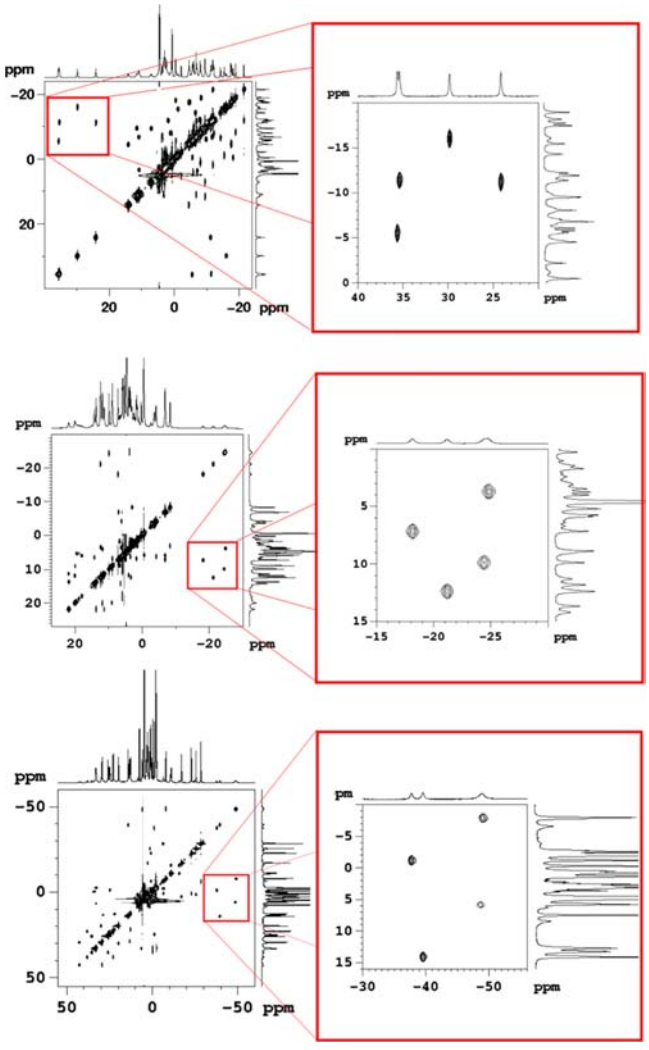

Figure 2. Homonuclear 2D-EXSY spectra acquired at 278 K and 14 T for EuHPDO3A (top), NdHPDO3A (middle), and PrHPDO3A (bottom).

The spectra have been assigned by taking advantage of the analogies with corresponding reported data on DOTA-like complexes (Table 1). EXSY spectra show the presence of cross peaks connecting axial (equatorial) protons of the SAP isomer and the equatorial (axial) protons of the TSAP form (Scheme 2). This result represents an unambiguous indication that the two diasteroisomers interconvert through the inversion of the macrocyclic ring.

However, the presence in the NMR spectra of two sets of signals does not necessarily imply the existence of only two diasteroisomers (two enantiomeric pairs). In fact, the presence of two sets of signals might be ascribed to the following:

dx.doi.org/10.1021/ic400716c | Inorg. Chem. 2013, 52, 7130−7138

Table 1. Proton NMR Peaks Assignment (278 K; pH = 7.0)

	PrHPDO3A δ (ppm)	NdHPDO3A δ (ppm)	EuHPDO3A δ (ppm)
ax_1 SAP	−37.6; −39.6; −48.6; −49.0	−24.8; −24.4; −21.1; −18.1	35.9; 35.8; 30.0; 24.5
ax_2 SAP	22.0; 28.8; 3 3.9; nd	19.4; 18.7; 17.9; 15.0	−15.1; −7.7; −11.5; −9.1
ax_1 TSAP	−17.1; −22.9; −25.6; −28.5	−8.3; −6.8; −6.9; −4.2	14.5; 11.9; 11.2; 11.2
ax_2 TSAP	24.8; 33.0; 33.1; nd	14.2; 12.4; 11.8; nd	−9.6; −17.1; −17.8; nd
eq_1 SAP	0.8; 1.0; 2.6; −6.5	7.1; 6.2; 5.8; 3.1	−4.2; −6.4; −9.1; 3.6;
eq_2 SAP	−2.6; 6.3; −0.3; −1.3;	6.4; 4.0; 3.4; nd	4.1; −0.1; −4.3; −5.7
eq_1 TSAP	−7.9; −1.2; −5.8; 14.1	12.4; 9.9; 7.2 ; 3.7	−5.1; −11.0; −15.3; −10.9
eq_2 TSAP	−0.3; 12.7; 13.3; nd	5.9; 5.2; 4.6; nd	−0.8; 1.5; 2.2; 7.4
$ac_{1,2}$ SAP	42.7; 38.0; 35.2; 29.8; 8.4; nd;	21.9; 21.8; 20.0; 19.9; 6.7; nd;	−1.8; −6.5; −21.1; −18.6; −11.8; −13.9;
$ac_{1,2}$TSAP	29.3; 25.8; 22.9; 19.7; 1.4; nd	13.7; 11.7; 11.3; 8.9; 8.8; nd	5.6; −6.2; −11.6; −7.98; −7.54; −11.4
-CH_3 SAP	nd.	5.8	1.0
-CH_3 TSAP	−2.0	−0.5	nd
-OH SAP	−25.3	nd	24.0
-OH TSAP	−28.8	−10	28.0
-CH SAP	−15.8	nd	nd
-CH TSAP	−11.1	nd	nd
-CH_2 SAP	nd	nd	nd
-CH_2 TSAP	nd	nd	nd

Scheme 2. Proton Labeling Scheme

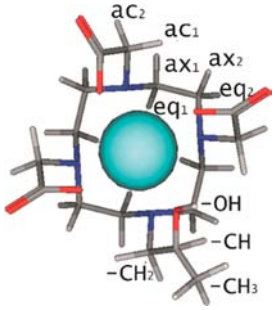

(i) the occurrence of a fast exchange between the SAP and TSAP forms of two pairs of diasteroisomers largely differing in their relative population. Since the EXSY spectra indicate that the dynamic process of ring inversion is slow (on the NMR time scale), it can be inferred that a fast exchange mechanism can only involve isomers interconverting through rotation of the arms (Scheme 1). This would result in exchange-averaged peaks arising from corresponding pairs of signals of SAP1 and TSAP1 (SAP2 and TSAP2). In addition, since the observed chemical shift values are quite typical of the TSAP and SAP forms, it can be deduced that the relative abundance of the rapidly interconverting isomer is very different;

(ii) an extremely low concentration of the remaining two enantiomeric pairs;

(iii) the presence in solution of just one diasteromeric pair in slow exchange on the NMR time scale that give rise to only two sets of signals, likely because the rotation of the arms is blocked.

To discriminate between these three different hypotheses, variable-temperature (278−350 K) ^{1}H NMR spectra of several LnHPDO3A complexes have been acquired and analyzed. For the heavier lanthanide ions (Ln = Tb, Dy, Ho, Er, Tm, and Yb), with increasing temperature above 298 K the signals of SAP broaden while those of TSAP get narrower (Figure 3).

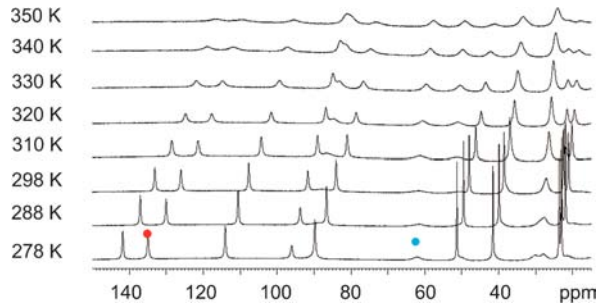

Figure 3. VT proton NMR spectra acquired at 14 T for YbHPDO3A. Two corresponding axial signals for SAP and TSAP are indicated with a circle (red = SAP, blue = TSAP).

This behavior indicates the occurrence of another dynamic process suggesting that all the 4 possible enantiomeric pairs are present. Furthermore, it can be inferred that the rotation of the pendant arms is faster than the inversion of the macrocyclic ring. This finding finds support in recent theoretical density functional theory (DFT) studies in combination with NMR data on the conformational dynamics of Ln(III) chelates with cyclen-based macrocyclic ligands.[33] The DFT calculations suggest for DO3A-derivatives a much lower activation free energy for the interconversion process through arm rotation than for ring inversion. The same conclusions cannot be drawn in the case of the lighter lanthanide ions (Ln = Pr, Nd, and Eu) since for both sets of signals the bandwidth increases with temperature.

All these observations lead to the conclusion that the first hypothesis is the most likely. In addition, it is reasonable to assume that the two most abundant diasteroisomers present in aqueous media are the same crystallographically independent molecules in the solid state, namely, $\Lambda(\lambda\lambda\lambda\lambda)$-*R* (TSAP-1*R*) and $\Lambda(\delta\delta\delta\delta)$-*R* (SAP-2*R*). Clearly, the presence of these two species in solutions also implies the presence of their enantiomers, $\Delta(\delta\delta\delta\delta)$-*S* (TSAP-2*S*) and $\Delta(\lambda\lambda\lambda\lambda)$-*S* (SAP-1*S*) (Scheme 3).

3.2. Solution Equilibria. Further relevant information can be gained by the measurement and analysis of the variation of the relative population of the diasteroisomers across the lanthanide series (Figure 4). These data can be obtained by measuring the area of the most downfield shifted NMR signals relating to the axial protons of the macrocycle.

In analogy with the DOTA chelates, the TSAP geometry is preferred at the beginning of the series because this structure provides a larger cavity to accommodate the larger ionic radius of early lanthanide(III) ions. On the other hand, the SAP isomer becomes increasingly more abundant until reaching a maximum for the Ho(III) ion. For heavier cations the mole fraction of SAP decreases with decreasing ionic radius. The comparable trend in the case of $[LnDOTA]^-$ complexes has been associated with the presence of a third species involved in the isomerization process that becomes more important with the contraction of the ionic radius. This third species showed a more contracted TSAP geometry in which the acetate arms are more strongly attracted toward the metal center, owing to the increased charge density on the lanthanide ion.[13] This geometry determines both a reduction of the cavity of the

dx.doi.org/10.1021/ic400716c | Inorg. Chem. 2013, 52, 7130−7138

Scheme 3. Diastereomeric Conform-ations of the Lanthanide Complexes of HPDO3A in Solution[a]

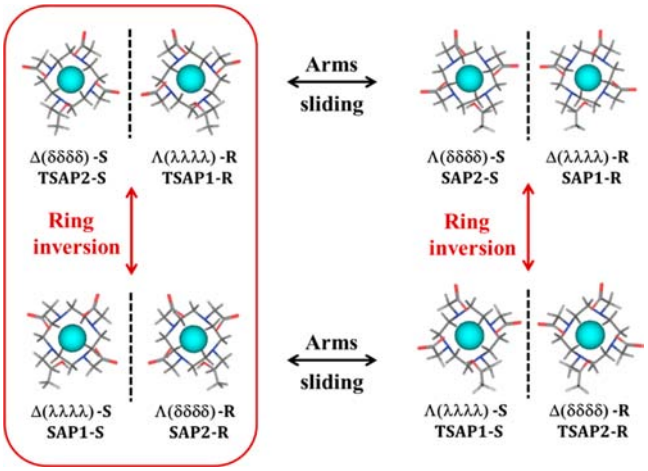

[a]On the left the most abundant species. Dashed lines represent the mirror plane.

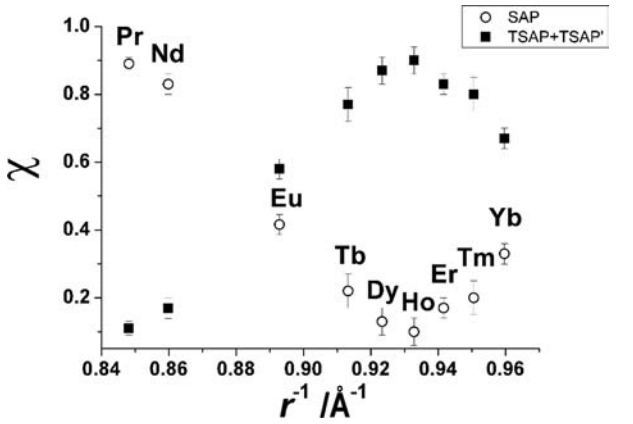

Figure 4. Molar fractions of the LnHPDO3A isomers measured at 298 K from the area of the NMR low-field axial peaks.

ligand and the loss of the bound water molecules because of an increased steric hindrance. This isomer has been referred to as TSAP′. It can be reasonably assumed that also in the case of LnHPDO3A chelates the presence of a tipping point around Ho(III) is due to the presence of the TSAP′ coordination geometry. By referring to the data of Figure 4, we make the obvious assumption that TSAP′ has an insignificant population at the beginning of the series (from La to Dy) whereas TSAP is negligible in the solutions of the late lanthanides (from Ho to Lu). The following equilibria have been considered:

$$\text{TSAP} \overset{K_1}{\leftrightarrow} \text{SAP} \tag{1}$$

$$\text{SAP} \overset{K_2}{\leftrightarrow} \text{TSAP}' + \text{H}_2\text{O} \tag{2}$$

where $K_1 = [\text{SAP}]/[\text{TSAP}]$; $K_2 = [\text{TSAP}']/[\text{SAP}]$.

The exchange between TSAP and SAP or between SAP and TSAP′ is slow on the NMR time scale as it is always possible to detect two distinct set of signals associated with these isomers at 298 K. Instead, the exchange between TSAP and TSAP′ is fast on the NMR time scale since only one set of signals that corresponds to the TSAP geometry is detected in the proton NMR spectra.

With the objective of obtaining a speciation diagram illustrating the variation of the relative population of the three isomers along the series of lanthanides, we have developed a model describing the molar fraction of SAP (Figure 4) as a function of the inverse of the ionic radius. To this aim we considered the following system

$$\begin{cases} K1 = [\text{SAP}]/[\text{TSAP}] \\ K2 = [\text{TSAP}']/[\text{SAP}] \\ C_\text{T} = [\text{SAP}] + [\text{TSAP}] + [\text{TSAP}'] \end{cases}$$

where C_T is the total concentration of the complex. From this system it is possible to derive the following equations

$$\chi_\text{SAP} = \frac{[\text{SAP}]}{C_\text{T}} = \frac{K_1}{1 + K_1 + K_1K_2} \tag{3}$$

$$\chi_{\text{TSAP}'} = \frac{[\text{TSAP}']}{C_\text{T}} = \chi_\text{SAP} \cdot K_2 = \frac{K_2K_1}{1 + K_1 + K_1K_2} \tag{4}$$

$$\chi_\text{TSAP} = \frac{[\text{TSAP}]}{C_\text{T}} = 1 - \chi_\text{SAP} - \chi_{\text{TSAP}'} = \frac{1}{1 + K_1 + K_1K_2} \tag{5}$$

where χ_SAP, χ_TSAP, and $\chi_{\text{TSAP}'}$ are the molar fractions of the SAP, TSAP, and TSAP′ isomers, respectively.

In the case of $[\text{LnDOTA}]^-$ chelates it has been found that the Gibbs free energy ΔG° for the isomerization process has a linear dependence on the inverse of the ionic radius, r.[13] By assuming the same behavior for the LnHPDO3A complexes, it is possible to express K_1 and K_2 as a function of r as follows

$$\ln K_1 = \frac{a_1}{r} + b_1 \rightarrow K_1 = \text{e}^{(a_1/r + b_1)} \tag{6}$$

$$\ln K_2 = \frac{a_2}{r} + b_2 \rightarrow K_2 = \text{e}^{(a_2/r + b_2)} \tag{7}$$

By substituting eqs 6 and 7 in eqs 3, 4, or 5, it is then possible to derive equations in which χ_SAP, $\chi_{\text{TSAP}'}$, and χ_TSAP are a function of $1/r$

$$\chi_\text{SAP} = \frac{\text{e}^{(a_1/r + b_1)}}{1 + \text{e}^{(a_1/r + b_1)} \times (1 + \text{e}^{(a_1/r + b_2)})} \tag{8}$$

$$\chi_{\text{TSAP}'} = \frac{\text{e}^{(a_1/r + b_1)} \times \text{e}^{(a_2/r + b_2)}}{1 + \text{e}^{(a_1/r + b_1)} \times (1 + \text{e}^{(a_2/r + b_2)})} \tag{9}$$

$$\chi_\text{TSAP} = \frac{1}{1 + \text{e}^{(a_1/r + b_1)} \times (1 + \text{e}^{(a_2/r + b_2)})} \tag{10}$$

χ_SAP has been experimentally determined by NMR (Figure 4), and the data have been fitted to eq 8 (Figure 5). The best fit procedure provides the slope a_1 and a_2 (54.9 ± 1.7 Å and 78.2 ± 1.4 Å) and the intercept b_1 and b_2 (−48.8 ± 1.5 and −75.8 ± 1.6). These, in turn, allow the determination of χ_TSAP and $\chi_{\text{TSAP}'}$ as a function of $1/r$ from eqs 9 and 10 (Figure 6).

It is clear from Figure 6 that the concentration of the TSAP′ diastereoisomer is negligible for the lighter lanthanides (Ce−Gd) as compared to the concentrations of the SAP and TSAP isomers. On the other hand, the population of TSAP form can be considered insignificant for the heavier lanthanides (Er−Yb). K_1 and K_2 are evaluated from the NMR peaks area for the isomeric species of only those lanthanide ions for which the

dx.doi.org/10.1021/ic400716c | Inorg. Chem. 2013, 52, 7130−7138

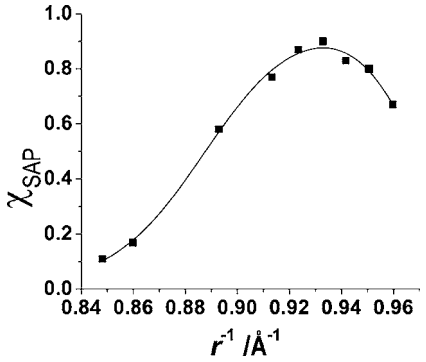

Figure 5. Experimental SAP molar fraction as a function of $1/r$ and calculated curve according to eq 8.

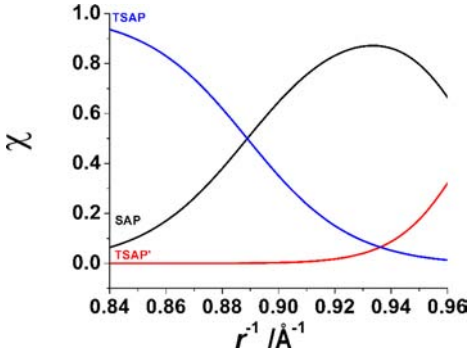

Figure 6. Speciation diagram according to eqs 8, 9, and 10.

population of the third isomer can be neglected (at the beginning or at the end of the series, respectively). The thermodynamic constants K_1 and K_2 enable the determination of the Gibbs free energy associated with the isomerization processes. In Figure 7 we plot the ΔG° values as a function of

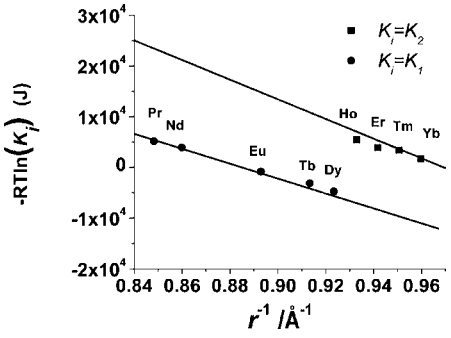

Figure 7. Gibbs free energy associated with the isomerization equilibria described by K_1 and K_2 as function of $1/r$ at 298 K.

$1/r$ with two simulated lines having $(-R\mathrm{Ta}_i)$ and $(-R\mathrm{Tb}_i)$ as slope and intercept. As expected, these lines interpolate quite well the ΔG° values only for Pr−Eu and Tm−Yb whereas for the lanthanides ions around the middle of the series (Tb−Er) deviations are observed that are accounted for by the occurrence of a significant population of a third isomer (TSAP′ or TSAP).

Further support to the validity of these conclusions is given by the analysis of the lanthanide induced NMR shift (LIS).[34] The LIS of the protons of each lanthanide complex depends on either through bond (contact shift) and through space interactions (pseudocontact or dipolar shift). The LIS can be conveniently expressed as a function of terms that are specific of the lanthanide ion and independent of the chelate ($\langle S_z\rangle$ and C_d) and of terms that depend only on the properties of the nucleus investigated (F and G). This allows a way to test the isostructurality of the chelates along the lanthanide series. Typically, the paramagnetic shift value, Δ, of a given nucleus for various complexes is plotted according to the following equations:

$$\frac{\Delta}{\langle S_z\rangle} = F + \frac{C_d}{\langle S_z\rangle}G \tag{11}$$

$$\frac{\Delta}{C_d} = G + \frac{\langle S_z\rangle}{C_d}F \tag{12}$$

In the presence of isostructurality of the LnHPDO3A complexes these plots should yield a straight line. On the contrary, a break in the linear behavior signals the occurrence of structural changes across the series. This analysis has been performed on the most shifted axial proton (ax_1) of the two isomeric species using eq 11 (Figure 8).

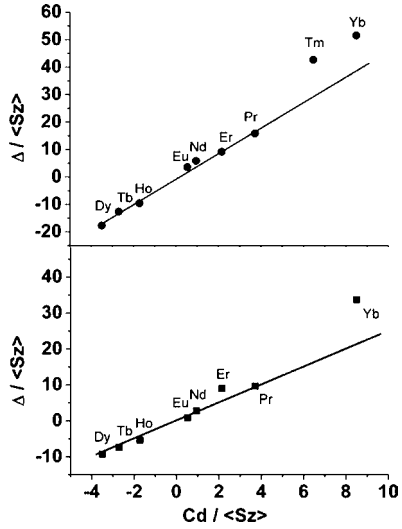

Figure 8. Plot of $\Delta/\langle S_Z\rangle$ vs $C_d/\langle S_Z\rangle$ for the axial proton (ax_1) of the SAP (top) and TSAP (bottom) isomeric forms.

Once again, a high degree of isostructurality is revealed for the SAP isomeric form, with the exception of Tm and Yb. Geometrical variations at the end of the series are often associated with the effect of the contraction of the ionic radius and could be indicative of the incipient presence of the SAP′ coordination geometry. In line with this hypothesis, the increasing population of TSAP′ is highlighted in the deviation from linearity of the LIS plot observed for the complexes of Er(III) and Yb(III).

3.3. Relaxometric Analysis. As mentioned above, the temperature dependence of the ^{17}O NMR transverse relaxation rate of GdHPDO3A, R_2, reveals an unusual trend at low temperatures and at high magnetic field strength (>9.4 T). Typically, for Gd(III)-chelates under an intermediate water exchange condition, R_2 increases by lowering the temperature, reaches a maximum value at around 300 K, and finally decreases at lower temperatures. This is the behavior reported for GdDTPA and GdDOTA that are characterized by a mean residence lifetime, τ_M, of the coordinated water molecule of about 300 ns at 298 K. On the other hand, in the case of

dx.doi.org/10.1021/ic400716c | Inorg. Chem. 2013, 52, 7130−7138

GdHPDO3A R_2 increases again for temperature values lower than about 280 K. Such a trend is barely visible at 11.7 T but becomes clearly observable at 14.1 T (Figure 9). This behavior

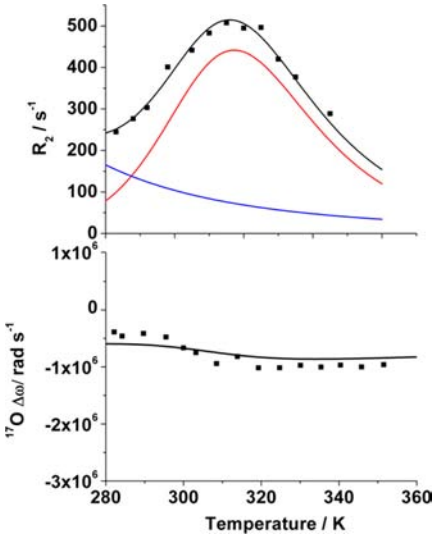

Figure 9. Top, transverse ^{17}O NMR relaxation rates as a function of temperature for GdHPDO3A recorded at 14.1 T. The red and blue lines represent the calculated contributions of the isomeric species SAP and TSAP, respectively. Bottom, 14.1 T ^{17}O NMR chemical shift as a function of temperature for GdHPDO3A.

could be associated with the presence in the aqueous solution of isomeric species with significantly different rates of water exchange ($k_{ex} = 1/\tau_M$). A quite similar hypothesis has been recently made on the basis of ab initio computer simulations that suggested a marked difference in the free-energies for the water exchange between two diastereoisomers of GdHPDO3A and highlighted the role of the network of hydrogen bonds that connect the inner- and the second solvation spheres.[21] We have then reanalyzed the ^{17}O NMR data (R_2 and shift, $\Delta\omega$) as a function of temperature and the ^1H nuclear magnetic relaxation dispersion (NMRD) profiles (at 10, 25, and 37 °C) by performing a global fitting in terms of a model that considers the presence in solution of two species whose relative population is extrapolated from the speciation diagram (χ = 0.7 and 0.3 for SAP and TSAP, respectively; Figure 6). The data could be well reproduced by considering a solution mixture of two isomeric forms (SAP and TSAP) characterized by quite similar rotational dynamics (τ_R = 65 ± 5 ps), water proton-gadolinium distance (r = 3.0 ± 0.2 Å), outer sphere relaxation parameters (a = 3.8 ± 0.1 Å; ^{228}D = 2.22 ± 0.2 × 10^5 cm^2 s^{-1}), scalar coupling constant ($A/\hbar$ = −3.5 ± 0.3 × 10^6 rad s^{-1}), and markedly differing in the electronic relaxation times (Δ^2 = 9.9 ± 0.5 and 1.5 ± 0.2 × 10^{19} s^{-2}; τ_V = 8 ± 1 and 30 ± 2 ps) and water exchange dynamics. The τ_R value obtained is entirely consistent with the values reported for strictly related complexes of analogous molecular volume.[35] In agreement with the computational study, for SAP the exchange lifetime value is rather long (τ_M = 640 ± 35 ns; E_M = 53 ± 8 kJ mol^{-1}) and fully comparable to those reported for other neutral Gd-chelates.[36,37] On the other hand, in TSAP τ_M assumes a value nearly 2 orders of magnitude shorter (τ_M = 8.9 ± 0.5 ns; E_M = 15 ± 2 kJ mol^{-1}). Looking at Figure 9, we can see that the contribution of the fast-exchanging species is almost negligible at physiological temperatures but becomes important for T < 290 K and predominant at lower temperatures. Clearly, it would not have been possible to highlight the presence of this species (TSAP) at lower values of magnetic field strength.

The influence of the isomeric mixture is less evident in the magnetic field dependency of the relaxivity (Figure 10).

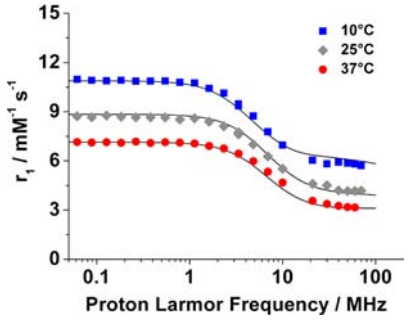

Figure 10. ^1H NMRD profiles of GdHPDO3A recorded at 10 (blue), 25 (gray) and 37 °C (red).

However, as mentioned above, the proton relaxivity of GdHPDO3A at 0.47 T and 298 K is slightly lower (∼ 4%) than the corresponding values for GdDOTA and GdDTPA. Although this difference may appear small, it is accentuated at lower temperatures to indicate that it is linked to the dynamics of the water exchange. Clearly, the exchange lifetime of the SAP isomer is long enough to limit the relaxivity at temperatures near 298 K and below. In fact, if the population of SAP changed from 70 to 20%, we calculate that the observed relaxivity of GdHPDO3A at 298 K would take the value of 4.8 mM^{-1} s^{-1}, the same as that of GdDTPA.

4. CONCLUSIONS

A detailed high resolution ^1H NMR study has revealed the presence of four enantiomeric pairs in the aqueous solutions of the lanthanide(III) complexes of HPDO3A. Two of these enantiomeric pairs are not directly detected in the high resolution NMR spectra because of their negligible relative abundance, and their presence is inferred from the analysis of the interconversion processes between the isomers. The chemical nature of the isomers has been elucidated on the basis of the new spectral data and of a crystallographic structure previously reported. The variation of the relative population of the SAP isomer along the lanthanide series has been measured from the NMR spectra. These data have represented the starting point for deriving a model that describes more thoroughly the molar fractions of the isomers as a function of the ionic radius. For the heavier members of the series a third isomeric form, lacking the bound water molecule, is also present in solution. The calculated molar fractions of the isomers of GdHPDO3A have been used to reanalyze the relaxometric data for this complex which enabled to explain its relaxivity value, slightly lower than expected, and the anomalous shape of the VT-^{17}O profile. A global fit of the data suggest that the TSAP form, present in lower concentration, is characterized by an extremely fast rate of water exchange which affects both the shape of the VT-^{17}O R_2 data and the amplitude of the ^1H NMRD profiles. Since it has been shown that in the case of DOTA derivatives it is possible to select a particular isomer through a suitable modification of the ligand, these results suggest that also in this case it is conceivable to chemically

dx.doi.org/10.1021/ic400716c | Inorg. Chem. 2013, 52, 7130−7138

control the population of the fast-exchanging isomeric species and optimize the relaxation efficacy of the Gd-complex.

AUTHOR INFORMATION

Corresponding Author

*E-mail: silvio.aime@unito.it (S.A.), mauro.botta@mfn.unipmn.it (M.B.). Phone: +39-011-6706451 (S.A.), +39 0131360253 (M.B.). Fax: +39-011-6706487 (S.A.), +39 0131360250 (M.B.).

Notes

The authors declare no competing financial interest.

ACKNOWLEDGMENTS

This research was supported by funding from University of Torino (code D15E11001710003), Regione Piemonte (PIIMDMT and Nano-IGT projects), MIUR (PRIN 2009), EU-FP7 integrated project ENCITE and ESF COST Action TD1004 (Theranostics Imaging and Therapy: An Action to Develop Novel Nanosized Systems for Imaging-Guided Drug Delivery). Scientific support from CIRCMSB (Consorzio Interuniversitario di Ricerca sulla Chimica dei Metalli nei Sistemi Biologici) is also gratefully acknowledged.

REFERENCES

(1) Caravan, P.; Ellison, J. J.; McMurry, T. J.; Lauffer, R. B. *Chem. Rev.* **1999**, *99* (9), 2293−2352.

(2) Aime, S.; Botta, M.; Terreno, E. *Adv. Inorg. Chem.* **2005**, *57*, 173−237.

(3) Muller, R. N.; Vander Elst, L.; Roch, A.; Peters, J. A.; Csajbok, E.; Gillis, P.; Gossuin, Y. *Adv. Inorg. Chem.* **2005**, *57*, 239−292.

(4) Delli Castelli, D.; Gianolio, E.; Geninatti Crich, S.; Terreno, E.; Aime, S. *Coord. Chem. Rev.* **2008**, *252* (21), 2424−2443.

(5) Parker, D.; Dickins, R. S.; Puschmann, H.; Crossland, C.; Howard, J. A. K. *Chem. Rev.* **2002**, *102*, 1977−2010.

(6) Aime, S.; Barge, A.; Botta, M.; Parker, D.; De Souse, A. S. *Angew. Chem., Int. Ed.* **1998**, *37*, 2673−267.

(7) Aime, S.; Barge, A.; Bruce, J. I.; Botta, M.; Howarth, J. A. K.; Moloney, J. M.; Parker, D.; De Souse, A. S.; Woods, M. *J. Am. Chem. Soc.* **1999**, *121*, 5762−5771.

(8) Congreve, A.; Parker, D.; Gianolio, E.; Botta, M. *Dalton Trans.* **2004**, *9*, 1441−1445.

(9) Geraldes, C. F. G. C.; Sherry, A. D.; Cacheris, W. P.; Kuan, K. T.; Brown, R. D., III.; Koenig, S. H.; Spiller, M. *Magn. Reson. Med.* **1988**, *8*, 191−199.

(10) Chang, C. A.; Brittain, H. G.; Telser, J.; Tweedle, M. F. *Inorg. Chem.* **1990**, *29*, 4468−4473.

(11) Alpoim, M. C.; Urbano, A. M.; Geraldes, C. F. G. C.; Peters, J. A. *J. Chem. Soc., Dalton Trans.* **1992**, 463−467.

(12) Jacques, V.; Desreux, J. F. *Inorg. Chem.* **1994**, *33*, 4048−4053.

(13) Aime, S.; Botta, M.; Fasano, M.; Marques, P. M.; Geraldes, C. F. G. C.; Pubanz, D.; Merbach, A. E. *Inorg. Chem.* **1997**, *36*, 2059−2068.

(14) Aime, S.; Barge, A.; Borel, A.; Botta, M.; Chemerisov, S.; Merbach, A.; Mu1ller, U.; Pubanz, D. *Inorg. Chem.* **1997**, *36*, 5104−5112.

(15) Terreno, E.; Botta, M.; Boniforte, P.; Bracco, C.; Milone, L.; Mondino, B.; Uggeri, F.; Aime, S. *Chem.—Eur. J.* **2005**, *11* (19), 5531−5537.

(16) Burai, L.; Jakab, S.; Kiraly, R.; Lazar, I.; Toth, I.; Brucher, E. *J. Chem. Soc., Dalton Trans.* **1996**, 1113.

(17) Sherry, A. D.; Ren, J.; Huskens, J.; Brucher, E.; Toth, E. A.; Geraldes, C. F. G. C.; Castro, M. M. C. A.; Cacheris, W. P. *Inorg. Chem.* **1996**, *35*, 4604.

(18) Pubanz, D.; Gonzhlez, G.; Powell, D. H.; Merbach, A. E. *Inorg. Chem.* **1995**, *34*, 4447−4453.

(19) Micskei, K. B.; Helm, L.; Brücher, E.; Merbach, A. E. *Inorg. Chem.* **1993**, *32*, 3844−3850.

(20) Delli Castelli, D.; Terreno, E.; Aime, S. *Angew. Chem., Int. Ed.* **2011**, *50* (8), 1798−800.

(21) Aime, S.; Delli Castelli, D.; Terreno, E. *Angew. Chem., Int. Ed.* **2005**, *44*, 5513−5515.

(22) Aime, S.; Delli Castelli, D.; Lawson, D.; Terreno, E. *J. Am. Chem. Soc.* **2007**, *129*, 2430−2431.

(23) Delli Castelli, D.; Terreno, E.; Cabella, C.; Chaabane, L.; Lanzardo, S.; Tei, L.; Visigalli, M.; Aime, S. *NMR Biomed.* **2009**, *22*, 1084−1092.

(24) Pollet, R.; Marx, D. *J. Chem. Phys.* **2007**, *126* (18), 181102.

(25) Pollet, R.; Nair, N. N.; Marx, D. *Inorg.Chem.* **2011**, *50*, 4791−4797.

(26) Corsi, D. M.; Platas-Iglesias, C.; van Bekkum, H.; Peters, A. J. *Magn. Reson. Chem.* **2001**, *39*, 723−726.

(27) Shannon, R. D. *Acta Crystallogr.* **1976**, *A32*, 751.

(28) Benetollo, F.; Bombieri, G.; Calabi, L.; Aime, S.; Botta, M. *Inorg. Chem.* **2003**, *42*, 148−157.

(29) Aime, S.; Botta, M.; Ermondi, G. *Inorg. Chem.* **1992**, *31*, 4291−4299.

(30) Woods, M.; Aime, S.; Botta, M.; Howard, J. A.; Moloney, J. M.; Navet, M.; Parker, D.; Port, M.; Rousseaux, O. *J. Am. Chem. Soc.* **2000**, *122*, 9781−9792.

(31) Jacques, V.; Desreux, J. F. *Inorg. Chem.* **1994**, *33*, 4048−4053.

(32) Kumar, K.; Allen, C.; Francesconi, L. C.; Dischino, D. D.; Malley, M. F.; Gougoutas, J. Z.; Tweedle, M. F. *Inorg. Chem.* **1994**, *33*, 3567−3575.

(33) Platas-Iglesias, C. *Eur. J. Inorg. Chem.* **2012**, *12*, 2023−2033.

(34) Peters, J. A.; Huskens, J.; Raber, D. J. *Prog. Nucl. Magn. Reson. Spectrosc.* **1996**, *28*, 283−350.

(35) Powell, D. H.; Dhubhghaill, O. M.; Pubanz, D.; Helm, L.; Lebedev, Y. S.; Schlaepfer, W.; Merbach, A. E. *J. Am. Chem. Soc.* **1996**, *118*, 9333−9346.

(36) Pintaske, J.; Martirosian, P.; Graf, H.; Erb, G.; Lodemann, K. P.; Claussen, C. D.; Schick, F. *Invest. Radiol.* **2006**, *41* (12), 859−859.

(37) Vogler, H.; Platzek, J.; Schuhmann-Giampieri, G.; Frenzel, T.; Weinmann, H. J.; Radüchel, B. *Eur. J. Radiol.* **1995**, *21* (1), 1−10.